Mesovortices, Polygonal Flow Patterns, and Rapid Pressure Falls in Hurricane-Like Vortices

JAMES P. KOSSIN AND WAYNE H. SCHUBERT

Department of Atmospheric Science, Colorado State University, Fort Collins, Colorado

(Manuscript received 21 July 2000, in final form 8 January 2001)

ABSTRACT

The present work considers the two-dimensional barotropic evolution of thin annular rings of enhanced vorticity embedded in nearly irrotational flow. Such initial conditions imitate the observed flows in intensifying hurricanes. Using a pseudospectral numerical model, it is found that these highly unstable annuli rapidly break down into a number of mesovortices. The mesovortices undergo merger processes with their neighbors and, depending on initial conditions, they can relax to a monopole or an asymmetric quasi-steady state. In the latter case, the mesovortices form a lattice rotating approximately as a solid body. The flows associated with such vorticity configurations consist of straight line segments that form a variety of persistent polygonal shapes.

Associated with each mesovortex is a local pressure perturbation, or mesolow. The magnitudes of the pressure perturbations can be large when the magnitude of the vorticity in the initial annulus is large. In cases where the mesovortices merge to form a monopole, dramatic central pressure falls are possible.

1. Introduction

The azimuthal mean tangential winds observed inside the radius of maximum tangential wind of hurricanes often exhibit a ''U-shaped'' profile (i.e., $\partial^2 v/\partial r^2 > 0$), while outside the radius of maximum wind, the mean tangential winds typically decrease significantly with radius (see, e.g., Willoughby et al. 1982, their Fig. 14). The symmetric part of the vorticity associated with such flows consists of an annular ring of enhanced vorticity in the eyewall with relatively weak vorticity inside (in the eye) and outside the eyewall.

A recent study by Schubert et al. (1999) suggested that the observed presence of polygonal features and mesovortices in hurricane eyewalls may be due to the emergence of asymmetric flows resulting from vorticity mixing. Working in an unforced two-dimensional (2D) barotropic framework, they numerically integrated an initial condition consisting of a barotropically unstable annulus of enhanced vorticity, and found that the annulus rolled up into four smaller vortices within ~5 h. As these ''mesovortices'' formed, the local flow around the eyewall and eye followed distinct straight line segments resembling observations of polygonal eyewalls. Within the following 6 h, the mesovortices lost their individual identities through merger processes, and the flow became more circular as mixing toward a monopole ensued. The relaxation toward a monopole occurred within 30–36 h and resulted in increased swirling flow near the vortex center, which caused a decrease in central pressure. In their experiment, the central pressure fall was approximately 9 mb.

The initial vortex used by Schubert et al. (1999) was large (120 km in diameter) and the annulus of enhanced vorticity was radially broad (30 km across). Montgomery et al. (2000) considered the 2D barotropic evolution of a similar, but smaller, vortex that could better represent the size and structure of observed mature hurricanes. They reduced the initial annulus used by Schubert et al. (1999) to 60-km diameter while reducing its radial width to 18 km and doubling its maximum vorticity. Numerical integration of this initial condition produced similar behavior to that noted by Schubert et al. (1999) but within a shorter time interval. For the initial conditions of Montgomery et al. (2000), relaxation to a monopole occurred within ~14 h, and the central pressure fall was ~12 mb.

While the initial conditions used by Montgomery et al. (2000) were chosen to be representative of mature hurricanes, evidence exists that intensifying hurricanes, such as those that typically exhibit mesovortices within or near their eyewalls, generally contain thinner annuli of enhanced vorticity in their eyewalls, and flow in the eye is often nearly irrotational. Emanuel (1997) provided theoretical evidence that the dynamics of the eyewall are frontogenetic and the local flow will tend toward a discontinuity. Using aircraft flight-level data, Kossin and Eastin (2001) found that during intensifi-

Corresponding author address: Dr. James P. Kossin, Department of Atmospheric Science, Colorado State University, Fort Collins, CO 80523.
E-mail: kossin@euler.atmos.colostate.edu

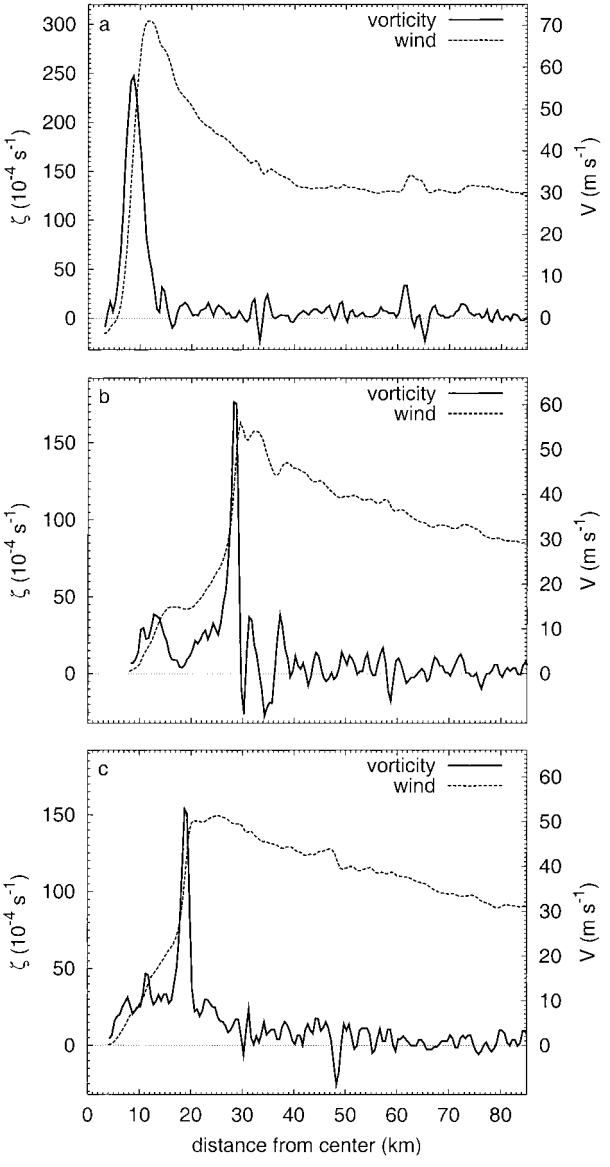

FIG. 1. Flight-level profiles of vorticity and tangential wind observed in (a) Hurricane Gilbert (1988) at 1934 UTC 13 Sep (700-mb pressure altitude), and Hurricane Guillermo (1997) at (b) 1935 UTC 2 Aug and (c) 4.5 h later. The wind profiles are U-shaped and the corresponding vorticity profiles can be described as thin annuli of strongly enhanced vorticity embedded in nearly irrotational flow. Tangential wind data are from the NOAA Hurricane Research Division archive.

cation, eyewall vorticity can become large within a thin annulus while vorticity near the eye center is nearly zero. Examples of such flows are shown in Fig. 1, which displays flight-level tangential wind and relative vorticity profiles observed by aircraft in Hurricanes Gilbert (1988) and Guillermo (1997). The vorticity profiles in Fig. 1 were calculated from the tangential wind profiles using a simple difference approximation of $\zeta(r) = \partial(rv)/r\partial r$.

The present work considers the evolution of very thin annular rings of enhanced vorticity in a 2D barotropic framework, and demonstrates that a number of features that emerge bear strong resemblance to features observed in intensifying hurricanes. In section 2a, we briefly discuss observational evidence for the existence of mesovortices and polygonal flow in the hurricane eyewall, and make general comparisons between idealized numerical results and observations. We find that under certain initial conditions, our numerical integrations produce mesovortices that are resistant to merger processes and can arrange themselves in persistent asymmetric configurations. Such resistance to merger has been well studied in the case of two corotating like-signed vortices (e.g., Moore and Saffman 1975; Saffman and Szeto 1980; Overman and Zabusky 1982; Griffiths and Hopfinger 1987; Melander et al. 1988; Carnevale et al. 1991a; Fine et al. 1991) and has recently been considered in the case of *n* vortices, which can emerge in electron plasma experiments and numerical simulations from unstable initial conditions, and subsequently arrange themselves into asymmetric equilibrium configurations (e.g., Fine et al. 1995; Jin and Dubin 1998; Schecter et al. 1999; Durkin and Fajans 2000).

In section 2b, we consider a case where the mesovortices eventually merge into a monopole at the vortex center and demonstrate that very large central pressure falls are possible simply in terms of vorticity rearrangement in the complete absence of moist physical processes. Section 2c addresses under what conditions a monopole will emerge and what conditions will most likely produce an asymmetric quasi-steady state. Sensitivity of the results to viscosity and model resolution will also be discussed.

2. Numerical results

Although boundary layer and moist processes certainly play an essential role in the evolutions of hurricanes, it is nevertheless meaningful to consider the role of conservative processes in the absence of additional physics. Such additional, and possibly extraneous, physics can obscure fundamental mechanisms, introduce parameterizations, and compromise numerical resolution and thus dynamical accuracy. With this in mind, we consider conservative (weakly dissipative) nonlinear vorticity dynamics using an unforced barotropic nondivergent model. The results presented in this work are thus highly idealized, and should be considered a single element in a hierarchal collection of past, present, and future modeling studies.

Radial profiles of vorticity in the near-core regions of hurricanes are sometimes observed to become fairly steep (Fig. 1), but they are nonetheless continuous, and thus our choice of numerical model should allow for continuous initial vorticity fields. Numerical models based on contour dynamics (e.g., Zabusky et al. 1979; Zabusky and Overman 1983), while offering the significant advantage of being able to model inviscid flows,

are limited to piecewise uniform initial vorticity fields. The evolution of such discontinuous vorticity fields, calculated using a contour reconnection–based dissipation scheme such as contour surgery (Dritschel 1988), can lead to persistent asymmetric shapes (Dritschel 1998), which would not emerge from continuous initial conditions.

Additionally, as discussed in Schubert et al. (1999), an initially unstable annulus of uniform vorticity with small undulations on its inner and outer contours can distort and evolve into a pattern in which the vorticity becomes ''pooled'' into rotating elliptical regions connected to each other by filaments or strands of high vorticity fluid. As the filaments become more and more intricately stretched and folded, contour dynamics/contour surgery adds more nodes to accurately follow the elongating contours, but also surgically removes fine-scale features. Surgical removal of vorticity during the simulation of a vorticity mixing process generally implies nonconservation of net circulation around the mixing region. As one of our goals is to characterize the ultimate end state of this process, we prefer a numerical method that preserves exactly the net circulation. We consequently employ a pseudospectral model with ordinary (∇^2) diffusion. Consequences of the inclusion of this type of diffusion, when modeling high Reynolds number geophysical flows, will be discussed in section 2c.

Numerical integrations are performed using the 2D barotropic pseudospectral model and generic initial conditions described by Schubert et al. (1999). In this model, vorticity evolution is described by

$$\frac{\partial \zeta}{\partial t} + \frac{\partial(\psi, \zeta)}{\partial(x, y)} = \nu \nabla^2 \zeta, \tag{1}$$

$$\nabla^2 \psi = \zeta. \tag{2}$$

Throughout the present work, unless otherwise noted, the model uses 512 $\times$ 512 collocation points on a 200 km $\times$ 200 km doubly cyclic Cartesian domain. After dealiasing, the effective resolution is 1.18 km. The value of viscosity is $\nu = 5\ \mathrm{m^2\ s^{-1}}$. The choice of ν is somewhat arbitrary in this model and is based on a compromise between increasing the Reynolds number and filtering high-wavenumber components in the vorticity field, a portion of which results from Gibb's phenomena that form as the vorticity gradients steepen, and palinstrophy increases, during the early part of the numerical integration. The time step Δt for each experiment, and additional information, is given in Table 1. The pressure field is diagnosed using the nonlinear balance equation

$$\frac{1}{\rho}\nabla^2 p = f\nabla^2 \psi + 2\left[\frac{\partial^2 \psi}{\partial x^2}\frac{\partial^2 \psi}{\partial y^2} - \left(\frac{\partial^2 \psi}{\partial x \partial y}\right)^2\right]. \tag{3}$$

This is a generalization of the gradient wind equation, to which it reduces in the axisymmetric case. In this work, we use $\rho = 1.13\ \mathrm{kg\ m^{-3}}$ and $f = 5 \times 10^{-5}\ \mathrm{s^{-1}}$.

As the initial condition for (1), we use $\zeta(r, \phi, 0) = \bar{\zeta}(r) + \zeta'(r, \phi)$, where $\bar{\zeta}(r)$ is an axisymmetric vorticity field and $\zeta'(r, \phi)$ is some small perturbation. Here, $\bar{\zeta}(r)$ is given by

$$\bar{\zeta}(r) = \begin{cases} \zeta_1, & 0 \le r \le r_1 \\ \zeta_1 S[(r - r_1)/(r_2 - r_1)] + \zeta_2 S[(r_2 - r)/(r_2 - r_1)], & r_1 \le r \le r_2 \\ \zeta_2 S[(r - r_2)/(r_3 - r_2)] + \zeta_1 S[(r_3 - r)/(r_3 - r_2)], & r_2 \le r \le r_3 \\ \zeta_1, & r_3 \le r \le r_4 \\ \zeta_1 S[(r - r_4)/(r_5 - r_4)] + \zeta_3 S[(r_5 - r)/(r_5 - r_4)], & r_4 \le r \le r_5 \\ \zeta_3, & r_5 \le r \end{cases} \tag{4}$$

where r_1, r_2, r_3, r_4, r_5, ζ_1, and ζ_2 are independently specified quantities, and $S(s) = 1 - 3s^2 + 2s^3$ is the basic cubic Hermite shape function. The constant ζ_3 is determined in order to make the domain average of $\zeta(r, \phi, 0)$ vanish. The initial perturbation $\zeta'(r, \phi)$ is imposed as proportional random noise (1% of the local vorticity or less) across the basic-state annulus. [Examples of initial profiles produced by (4) are shown by the solid lines in Figs. 3, 7, and 11.]

a. Mesovortices and polygonal flow

Mesovortices are sometimes observed in and around the eyewalls of intense hurricanes and have been documented in a number of studies (Fletcher et al. 1961; Marks and Houze 1984; Muramatsu 1986; Bluestein and Marks 1987; Black and Marks 1991; Willoughby and Black 1996). As suggested by Marks and Black (1990), the occurrence of mesovortices is probably more common than previously believed. As shown by Black and Marks (1991), mesovortices are associated with local wind and pressure perturbations. For the case of a mesovortex encountered at the inner eyewall edge in Hurricane Hugo (1989), they measured tangential winds that changed 57 m $\mathrm{s^{-1}}$ in a radial distance of about 0.5 km, resulting in vorticity values greater than 1000 $\times$ 10^{-4} $\mathrm{s^{-1}}$, and they found an associated pressure minimum

TABLE 1. Description of expts. 1–9. Columns 2, 3, and 4 display initial values of the maximum eyewall vorticity, maximum tangential wind, and radius of maximum tangential wind (RMW), respectively. Column 5 shows the maximum pressure fall achieved during the numerical integration. Column 6 shows the time step used in the model.

Expt. No.	$(\zeta_{max})_{t=0}$ (10^{-4} s^{-1})	$(v_{max})_{t=0}$ (m s^{-1})	$(RMW)_{t=0}$ (km)	Pressure fall (mb)	Δt (s)	Comments
1	249	45	17	14	5	Relaxes to crystal
2	249	43	12	15	5	Relaxes to monopole
3	225	39	12	11	7.5	Relaxes to monopole
4	338	58	12	28	5	Relaxes to tripole
5	448	77	12	49	3	Relaxes to monopole
6	395	74	33	51	3	Chaotic mesovortex motions
7	248	75	13	32	3	Radially broader annulus; relaxes to monopole
8	249	43	12	13	5	Same as expt. 2 but with ν increased from 5 to 25 m^2 s^{-1}
9	249	43	12	15	2.5	Same as expt. 2 but at twice finer spatial resolution and $\nu = 1.25$ m^2 s^{-1}

that was actually lower than the pressure measured near the eye center.

Another interesting feature that has been observed in the region of the hurricane eyewall is the presence of ''polygonal'' patterns in radar reflectivity (Lewis and Hawkins 1982; Muramatsu 1986). The shapes range from triangles to hexagons and, while they are often incomplete, straight line segments can often be identified. Scrutiny of airborne radar images suggests that the presence of straight line segments in eyewall reflectivity is not a rare occurrence. Examples of this can be seen in Fig. 2, which depicts aircraft measured radar reflectivity in Hurricanes Guillermo (1997) and Bret (1999) during rapid intensification. The features in Guillermo shown in Fig. 2 were evident within a deep layer (2700–6100-m altitude).

As the initial condition for the first numerical experiment (expt. 1), we choose $r_1 = 13$ km, $r_2 = 15$ km, $r_3 = 17$ km, $r_4 = 35$ km, $r_5 = 45$ km, $\zeta_1 = 1.02 \times 10^{-4}$ s^{-1}, $\zeta_2 = 248.52 \times 10^{-4}$ s^{-1}, and $\zeta_3 = -1.48 \times 10^{-4}$ s^{-1}, which describe a vortex with maximum tangential wind of 45 m s^{-1} located near $r = 17$ km (Table 1 and Fig. 3). Inside $r = 13$ km, the tangential wind is nearly zero and the profile is nearly flat. The minimum pressure perturbation[1] calculated using (3) is -14.3 mb located at the vortex center, and the pressure profile is roughly flat inside $r = 15$ km.

Results of expt. 1 are shown in Fig. 4. Figure 4a depicts 2D maps of vorticity with superimposed wind vectors. Figure 4b shows 2D maps of pressure perturbation with superimposed contours of streamfunction ψ. The unstable initial vortex quickly rolls up into eight mesovortices that subsequently undergo rapid mergers. At $t = 0.45$ h, just prior to rollup, an azimuthal wavenumber eight instability is evident. The growth of the perturbations to finite amplitude is a generic feature of the early evolution of unstable annuli, and results in vorticity fields that bear resemblance to observed radar reflectivity fields. This can be seen by comparison of the vorticity at $t = 0.45$ h with Fig. 2a. The interface between low and high reflectivity measured in Guillermo's eye and eyewall, respectively, exhibits wavelike perturbations from axisymmetry while small localized regions of enhanced reflectivity are evident in the eyewall.

At $t = 1.75$ h (not shown), five mesovortices remain and are maintained for the following 4 h of integration. Each mesovortex is associated with a local pressure perturbation. These perturbations fluctuate as the mesovortices change their configuration relative to each other while orbiting cyclonically about their centroid. During the numerical integration, the minimum pressure perturbation associated with a mesovortex was -28.5 mb, or about twice the initial perturbation minimum.

At $t = 3.5$ h, the streamlines follow a number of straight line segments that roughly form a pentagon. This pentagonal flow emerged at $t = 1.75$ h, and was maintained for 4 h until a final merger took place at $t \approx 6$ h. After the final merger at $t = 6$ h, the flow pattern resembles a square and remains essentially unchanged during the following 18 h. In our idealized framework, in which diabatic and frictional forcing have been neglected, this square configuration of the mesovortices could exist indefinitely in the absence of viscosity; that is, the mesovortices form a rigid lattice that rotates as a solid body. Such asymmetric steady (nonergodic) solutions have been identified in laboratory experiments using electron plasmas, and have been named ''vortex crystals'' (Fine et al. 1995; Jin and Dubin 1998; Schecter et al. 1999; Durkin and Fajans 2000). It is interesting to note that, due to the less than perfect 2D nature of the plasmas, experimental simulations initialized with unstable hollow annular electron plasmas can produce erroneous equilibrium solutions, consisting of broader stable annuli, when the initial annuli are comparably thin to the initial conditions of the present work (Peurrung and Fajans 1993).

Schecter et al. (1999) also identified vortex crystals in vortex-in-cell simulations. To the best of our knowledge, our results show the first documented case of vortex crystal formation in a pseudospectral numerical integration. The stability of such asymmetric equilibrium configurations has been the subject of numerous pre-

[1] The pressure perturbation is defined by $\Delta p = p - p_{far}$, where p_{far} is the pressure at $r = 100$ km.

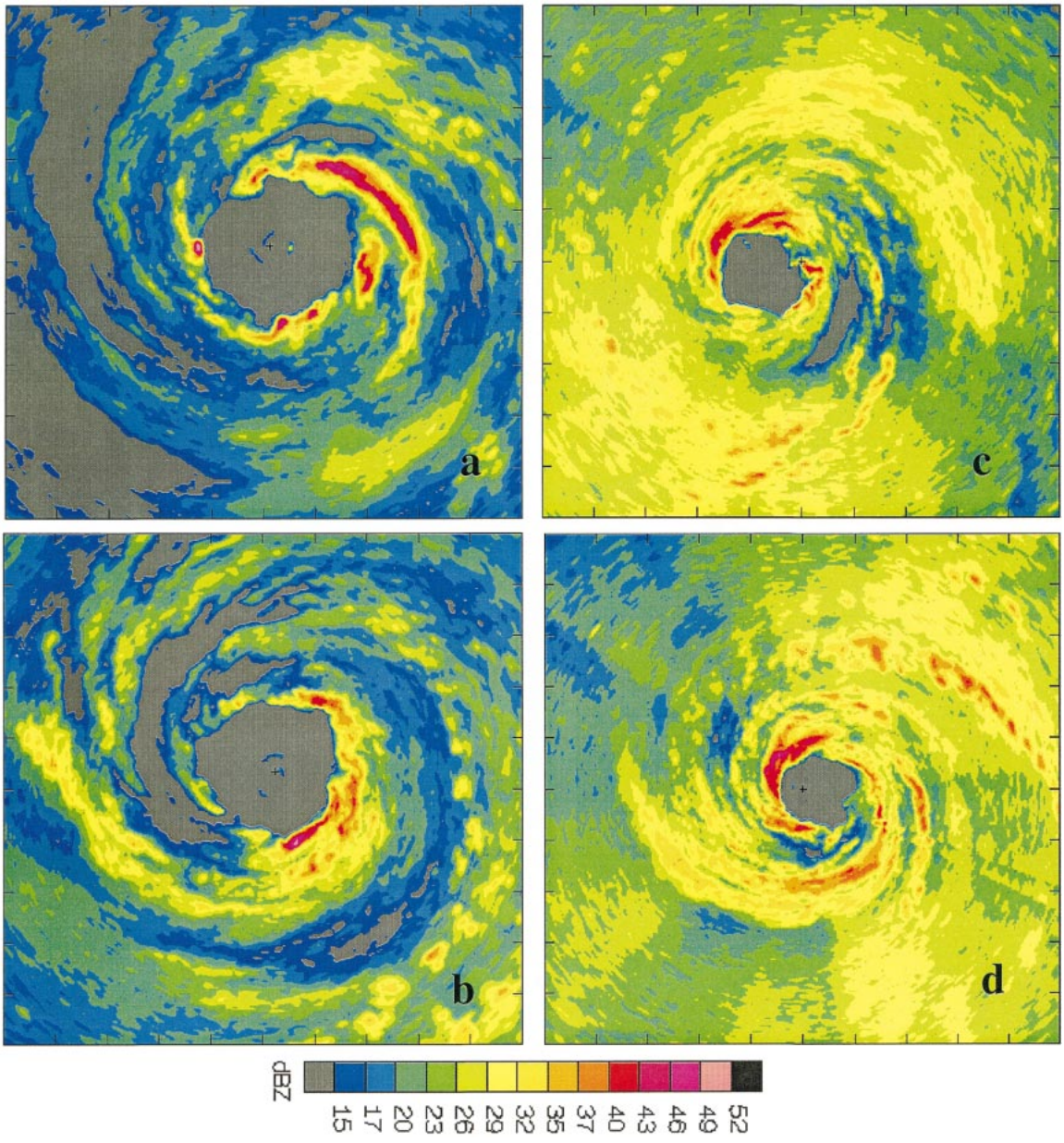

FIG. 2. Airborne-radar reflectivity in Hurricanes Guillermo (1997) (left panels) and Bret (1999) (right panels). The small crosses near the eye center denote the position of the aircraft. (a) 180 km × 180 km reflectivity field at 1935 UTC 2 Aug (corresponding with Fig. 1b). Aircraft altitude was 5527 m. At this time Guillermo was rapidly intensifying from a category 1 to a category 3 storm as the central pressure was falling at a rate of 4 mb h^{-1}. Note the wavelike irregular pattern along the inner edge of the eyewall. (b) 180 km × 180 km reflectivity 4.5 h later at 6134-m altitude (corresponding with Fig. 1c). Note the distinct straight line segments along the inner edge of the eyewall. Straight line segments evident in 240 km × 240 km reflectivity fields in Bret at (c) 2022 UTC (4164-m altitude) and (d) 2251 UTC 21 Aug (4267-m altitude), just prior to the onset of rapid intensification. (Images courtesy of NOAA Hurricane Research Division.)

vious studies (e.g., Thomson 1883; Havelock 1941; Stewart 1943; Morikawa and Swenson 1971; Dritschel 1985). An excellent summary of this body of work can be found in Persing and Montgomery (1995).

As demonstrated in Fig. 2, the interface between eye and eyewall reflectivity measured in hurricanes can consist of a number of straight line segments that give the eyes a polygonal appearance. The reflectivity is a measure of the shape of a mass of particles (raindrops) that are falling through a background flow at their relative terminal velocities. The flow associated with the persistent mesovortex configuration of expt. 1 would result in a similar reflectivity field. This is demonstrated in Fig. 5, which shows that initially concentric rings of passive tracers are convoluted into a number of straight line segments by the presence of persistent mesovorti-

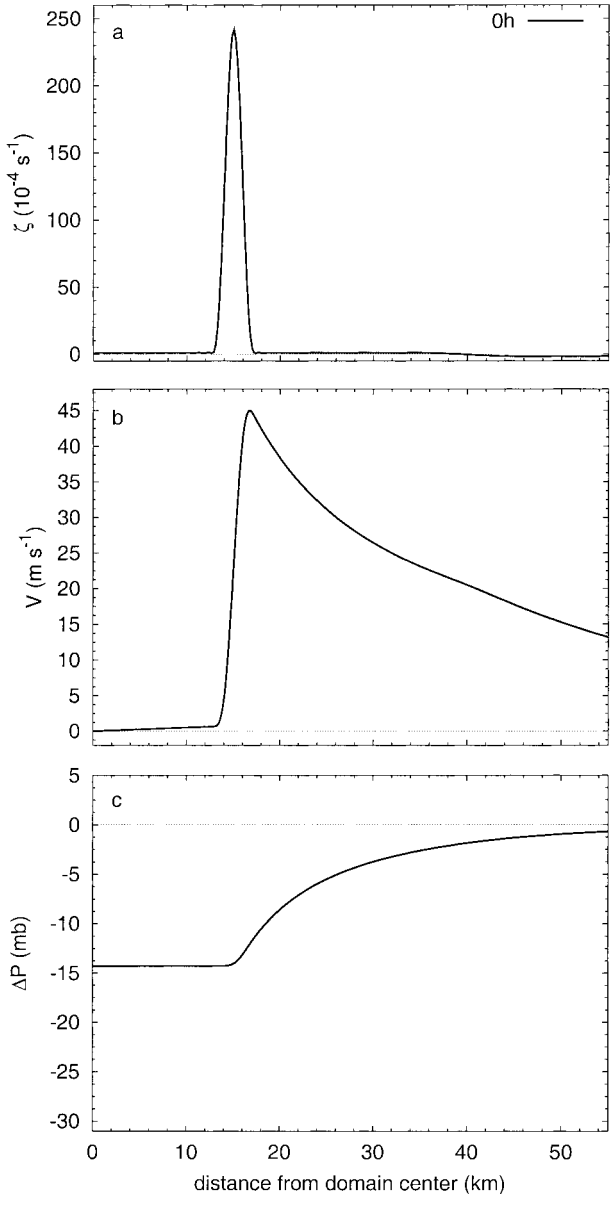

FIG. 3. Initial conditions for expt. 1: (a) vorticity, (b) tangential wind, and (c) pressure perturbation.

ces. The straight line segments are separated by ''kinks'' in the tracer field and are especially evident inside the annular region containing the mesovortices, that is, near the eye–eyewall interface. Each kink is located slightly upwind of a mesovortex. The kinks that were evident in the reflectivity fields shown in Fig. 2 were typically located slightly upwind of local maxima of reflectivity. This suggests that small localized regions of enhanced convection are collocated with local vorticity maxima.

Flows such as those shown in Fig. 4 raise the question of how a vortex *center* should be defined. Comparison of pressure perturbations with streamfunction shows that there can be multiple pressure centers (i.e., points of minimum pressure) and it is also possible to have multiple wind centers (i.e., points of zero tangential wind) even with respect to a nonrotating frame of reference. For example, in Fig. 4a at $t = 3.5$ h, a closed circulation is seen in the wind vectors around the mesovortex in the northwest quadrant. The wind centers are not collocated with the pressure minima, and none of the wind nor the pressure centers are collocated with the domain center.

b. Central pressure falls

In section 2a, we noted that mesovortices can be associated with significant pressure perturbations. In a group of experiments, where the diameters and radial spans of the initial annuli were varied, we found a number of evolutions ranging from a variety of vortex crystal formations to rapid collapse to a monopole. The pressure perturbations associated with the mesovortices were generally large provided that the vorticity in the initial annulus was large. In cases of monopole formation, the ''central'' pressure perturbations can be especially large as relatively strong vorticity consolidates at the domain center.

For the second experiment (expt. 2), the model is initialized using $r_1 = 8$ km, $r_2 = 10$ km, $r_3 = 12$ km, $r_4 = 30$ km, $r_5 = 40$ km, $\zeta_1 = 1.48 \times 10^{-4}$ s^{-1}, $\zeta_2 = 248.98 \times 10^{-4}$ s^{-1}, and $\zeta_3 = -1.02 \times 10^{-4}$ s^{-1}. This vortex is similar to the initial condition used in expt. 1, but the radius of maximum wind is shifted 5 km inward to $r \approx 12$ km. The maximum wind is 43 m s^{-1} and the minimum pressure perturbation is -14.4 mb located at the center of the annulus.

Results of expt. 2 are shown in Fig. 6. Within 0.75 h, the annulus rolls up into six mesovortices, which quickly merge to form five mesovortices in the following 0.5 h. At $t = 1.5$ h, the minimum pressure perturbation (-24 mb) is associated with the mesovortex located in the eastern quadrant. The mesovortex located in the northern quadrant is associated with a weak pressure perturbation, but its presence is distinctly evident in the streamfunction contours, and straight line flow segments are seen in the northeast and northwest quadrants. This mesovortex configuration is maintained until $t \approx 2.75$ h, when a final merger event consolidates the vorticity into a monopole over the following 1 h. After the final merger, the central pressure perturbation is -29 mb, which demonstrates a decrease in central pressure of 15 mb in about 4.5 h, or ~ 3.3 mb h^{-1}.

Azimuthally averaged cross sections of vorticity, tangential wind, and pressure perturbation at $t = 0$ h and $t = 10$ h are shown in Fig. 7. At $t = 10$ h, the maximum average vorticity near the domain center is 213×10^{-4} s^{-1}, which demonstrates the ability of the mesovortices to transport vorticity from the initial annulus to the center of the final monopole, while protecting the high vorticity in their cores (e.g., Carnevale et al. 1991b; Bracco et al. 2000) from mixing with the surrounding irrota-

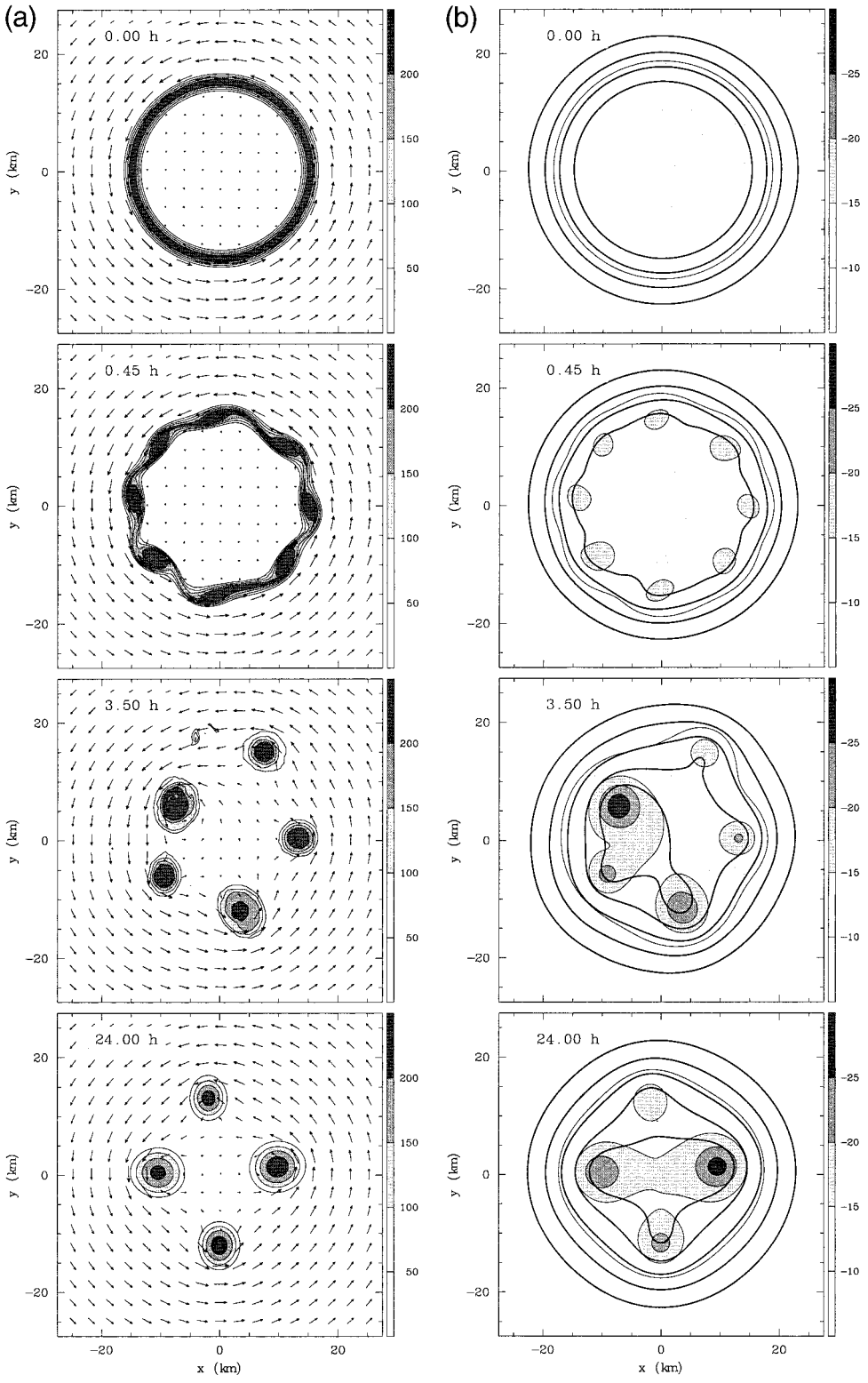

FIG. 4. (a) Vorticity contour plots and (u, v) wind vectors for expt. 1. The model domain is 200 km × 200 km but only the inner 55 km × 55 km is shown. The contours begin at 50×10^{-4} s^{-1} and are incremented by 50×10^{-4} s^{-1}. Values along the label bar are in units of 10^{-4} s^{-1}. Darker shading is associated with higher values of vorticity. (b) Pressure perturbation contour plots with contours of streamfunction (bold contours) superimposed. (Values along the label bar are in mb. Model run time in hours is shown on each plot.)

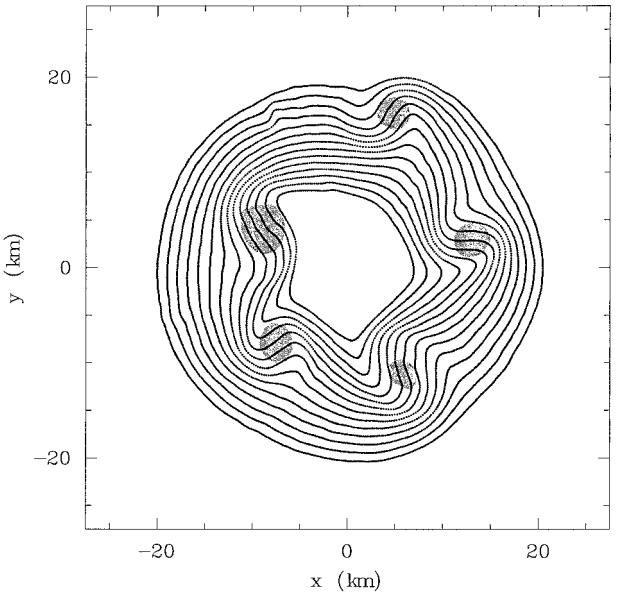

FIG. 5. Convolution of initially concentric rings of passive tracers due to the presence of mesovortices in an eyewall. The rings of tracers were placed into the flow shown in Fig. 4 at $t = 3.5$ h and were advected for 5 min. The mesovortices are identified by the small gray shaded areas. The straight line segments are separated by kinks that are always located slightly upwind of the mesovortices.

tional fluid. As high vorticity is transported inward, the tangential winds inside $r \approx 10$ km increase considerably. For example, the flow near $r = 5$ km increases from 0.3 to 33 m s^{-1}. The radius of maximum wind contracts from $r = 12$ km to $r = 5.2$ km. This dramatic contraction marks a new result in comparison with the results of Schubert et al. (1999) and Montgomery et al. (2000) that showed very little change in the position of the radius of maximum wind during relaxation to a monopole. Note that although the radius of maximum wind contracts, and the central pressure has fallen 15 mb, the maximum wind decreases 10 m s^{-1}. Such flow evolutions emphasize the inherent uncertainty in empirical pressure–wind relations that ignore the potential vorticity structure of the vortex.

In similar experiments, in which the maximum vorticity in the initial annulus was varied, we found that stronger vortices exhibited similar behavior, but the central pressure falls could be much larger. To demonstrate this, we integrated three initial vortices with annuli of the same size and radial width as expt. 2, but with differing vorticity maxima. These are listed as expts. 3, 4, and 5 in Table 1. Figure 8 displays the evolution of $\Delta p_{\min}$ for expts. 2, 3, 4, and 5, where $\Delta p_{\min}$ is the minimum pressure perturbation in the model domain at time t.

As seen in each of the curves in Fig. 8, during the early part of the evolution, $\Delta p_{\min}$ decreases as the annulus rolls up into a number of mesovortices, and subsequent mergers and configuration changes of the mesovortices cause $\Delta p_{\min}$ to fluctuate slightly. The final merger results in a final decrease of $\Delta p_{\min}$. For expt. 3, the initial condition relaxed to a monopole within 5 h and the central pressure fall was 11 mb. For expt. 4, within 11 h of numerical integration, all of the high vorticity originally in the annulus was consolidated at the center. In this case, the annulus relaxed to a tripole and the equilibrated central vorticity was elliptical [for further discussion regarding tripoles, see Kossin et al. (2000) and references cited therein]. The central pressure fall was 28 mb. For expt. 5, a monopole was formed within 13 h, and *the central pressure fall was 49 mb.* Thus, if asymmetric vorticity mixing was proposed as a mechanism to explain the onset of intensification, it could be argued that the observed presence of a thin ring of strongly enhanced vorticity in a hurricane eyewall may be a precursor to rapid and large central pressure falls, while weaker vorticity in the eyewall may be a precursor to rapid, but smaller pressure falls.

c. Two extreme cases

Experiments 2, 3, 4, and 5 relaxed to monopolar (or tripolar) vorticity fields, while the larger annulus of expt. 1 relaxed to an asymmetric quasi-steady vortex crystal state. In a larger group of experiments, we found that, in agreement with previous electron plasma experiments (e.g., Peurrung and Fajans 1993), monopoles were more likely to form from smaller or radially broader initial annuli, while asymmetric vortex crystal solutions were most likely to emerge from the largest and thinnest annuli. For a given radial width, larger annuli are unstable to higher azimuthal wavenumbers and roll up into larger numbers of mesovortices. After the initial period of merger events, the remaining mesovortices are apparently resistant to further merger, although the configurations can change chaotically.

To illustrate these points, we now consider the evolution of two initial conditions. For the first (expt. 6), we expand the annulus used in expt. 1 to a ~60-km diameter, and we increase the maximum vorticity of the annulus to 395×10^{-4} s^{-1}. The initial maximum wind is 74 m s^{-1}, located at $r = 33$ km. Results of expt. 6 are shown in Fig. 9 in the form of vorticity maps with superimposed contours of streamfunction. At $t = 0.5$ h, the annulus has rolled up into 13 mesovortices which rapidly merge within the following 0.5 h to form 8 mesovortices. Two additional mergers take place at $t = 4.5$ h, resulting in six mesovortices. Although these six mesovortices are resistant to further merger, they do not quickly relax into a steady vortex crystal. Instead they undergo chaotic movements that result in a number of polygonal streamline shapes. If merger were the only process operating, we might expect hurricane eyewalls to always transition to polygons with fewer sides. However, the chaotic behavior of the mesovortex positions may also be important. For example, as illustrated in Fig. 9 at $t = 12$ and 15 h, it is possible for one of the mesovortices to migrate to the center, remain there for a few hours, and then migrate back, causing the eyewall

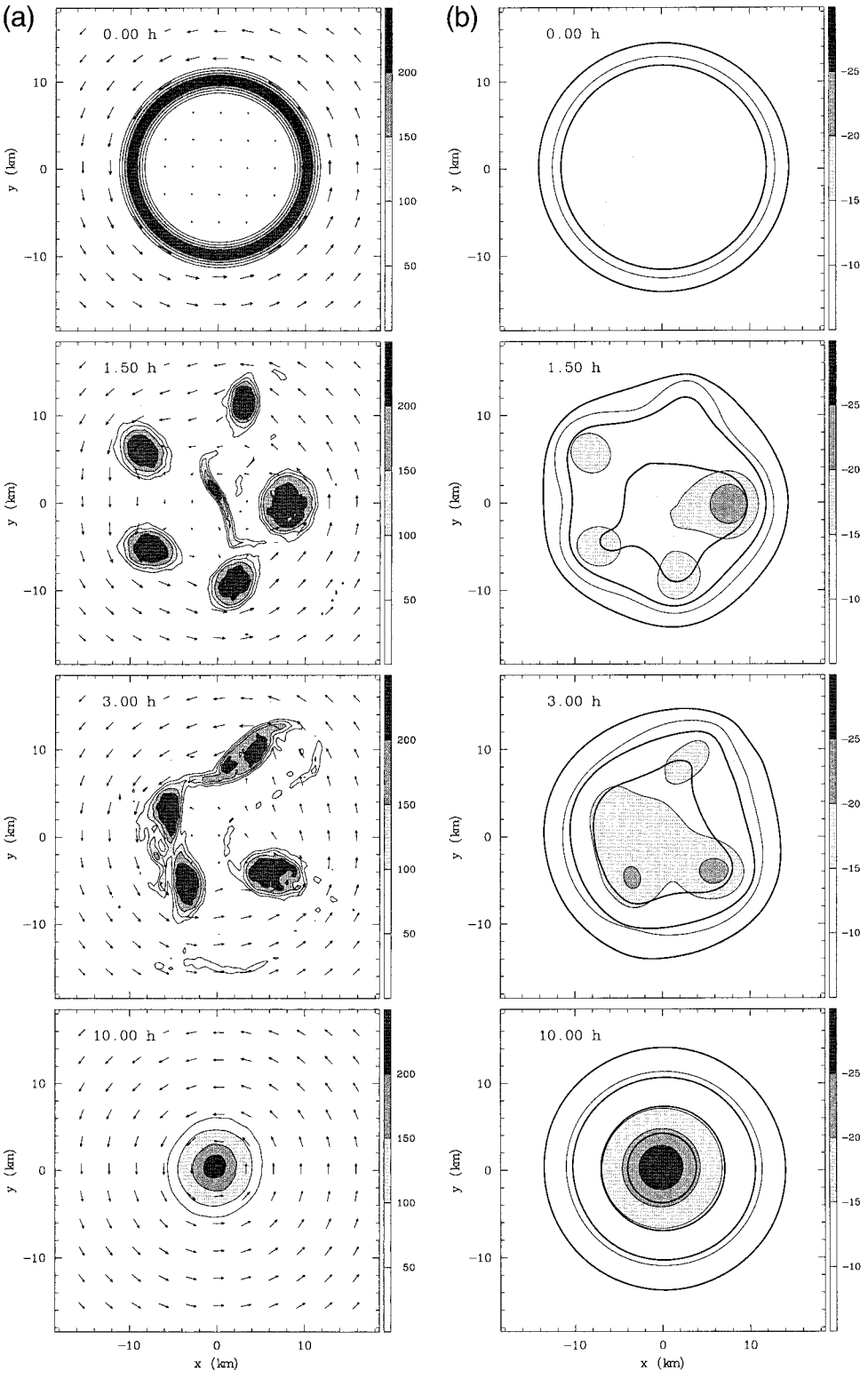

FIG. 6. Similar to Fig. 4, but for expt. 2. The model domain is 200 km × 200 km, but here only the inner 37 km × 37 km is shown.

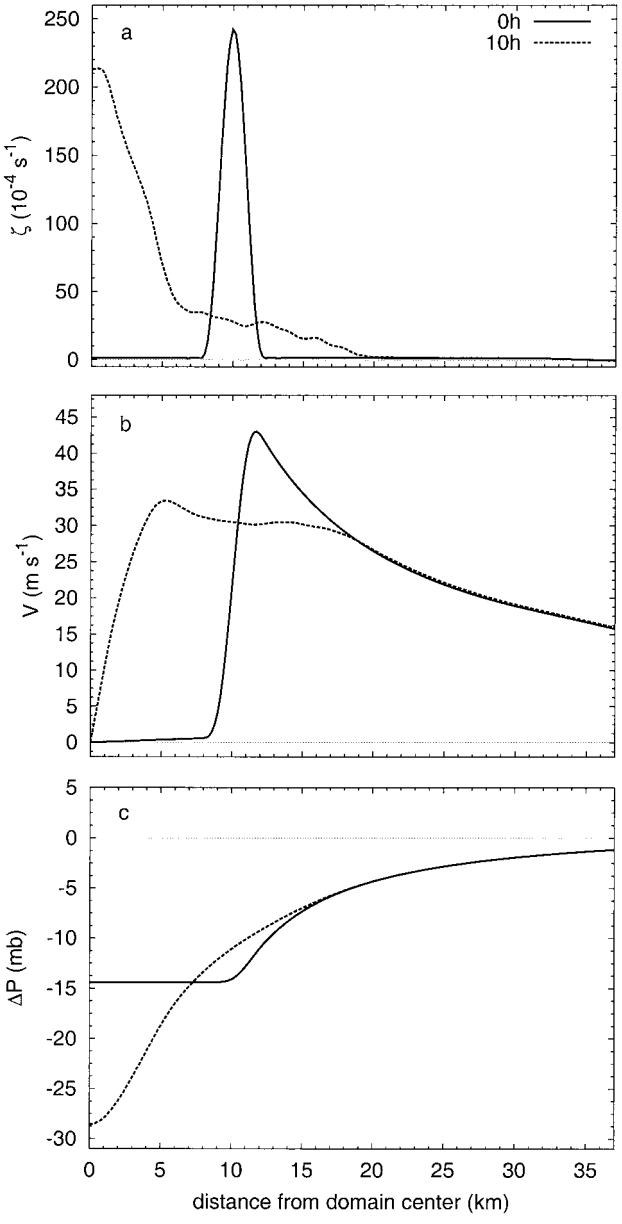

FIG. 7. Azimuthal mean (a) vorticity, (b) tangential velocity, and (c) pressure perturbation for expt. 2 at the selected times $t = 0$ (solid) and 10 h (dashed). Averages were computed with respect to distance from the domain center. The pressure perturbation Δp is fixed at zero at $r = 100$ km.

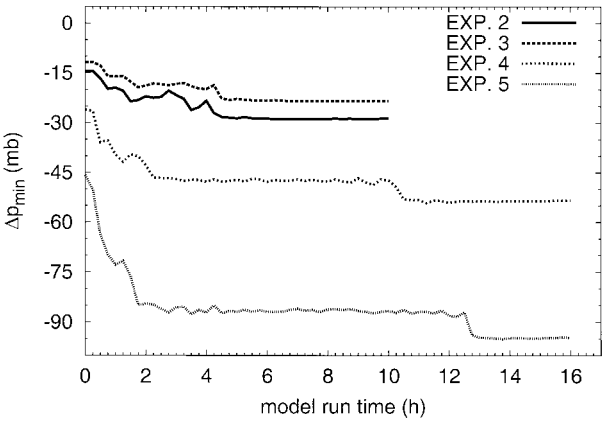

FIG. 8. Time evolution of $\Delta p_{\min}$ for expts. 2, 3, 4, and 5.

streamline pattern to transition from a pentagon to a hexagon. A subsequent transition from a hexagon to a pentagon, with no associated merger event, occurs between $t = 15$ and 18 h. Thus, if both merger processes and chaotic mesovortex movements are important, perhaps all we can say is that transitions to polygons with fewer sides are more likely than the reverse.

For the next experiment (expt. 7), we initialize the model using $r_1 = 6$ km, $r_2 = 10$ km, $r_3 = 14$ km, $r_4 = 30$ km, $r_5 = 40$ km, $\zeta_1 = 0.703 \times 10^{-4}\ \mathrm{s}^{-1}$, $\zeta_2 = 248.203 \times 10^{-4}\ \mathrm{s}^{-1}$, and $\zeta_3 = -1.797 \times 10^{-4}\ \mathrm{s}^{-1}$. This vortex is similar to the initial condition of expt. 2, but the annulus is radially broader and the resulting maximum wind is greater. The maximum wind is 75 m s^{-1}, located at $r = 13$ km, and the minimum pressure perturbation is -48 mb located at the center of the annulus. Figure 10 shows the evolution of this initial vortex in the form of vorticity maps, and Fig. 11 shows initial and final azimuthal mean profiles of vorticity, tangential wind, and pressure perturbation. At $t = 1$ h, the annulus has rolled up into four mesovortices. The size of the mesovortices and the proximity of their neighbors result in a deformation field that induces rapid merger, and at $t = 2$ h, all mesovortices have lost their individual identities. The equilibrated monopole evident at $t = 8$ h, has 60 m s^{-1} maximum wind located near the initial radius of maximum wind. The central pressure fall in 8 h is 32 mb.

In addition to the diameter and thickness of the annulus, the strength of the central, or eye, vorticity plays an important role in whether a monopole rapidly forms and how large a pressure fall can be realized through the mixing process. The presence of substantial central vorticity affects the evolution in two ways. First, the central pressure of the initial vortex will be lower due to stronger local winds in the eye. The relaxation of an unstable annulus to a monopole will then cause a smaller central pressure fall since the winds in the eye will not increase as much. Second, the presence of substantial central vorticity imposes a deformation across the mesovortices which emerge from the annulus (in the eyewall). This deformation apparently makes the mesovortices less resistant to merger.

Schubert et al. (1999) studied the linear stability of annular rings of enhanced vorticity in the simplified context of piecewise uniform vorticity profiles. They were thus able to reduce their analyses to a 2-parameter space (δ, γ), where δ was related to the diameter and radial thickness of the annulus, and γ was related to a ratio of the depressed central vorticity and the enhanced vorticity in the annulus. This is essentially the parameter

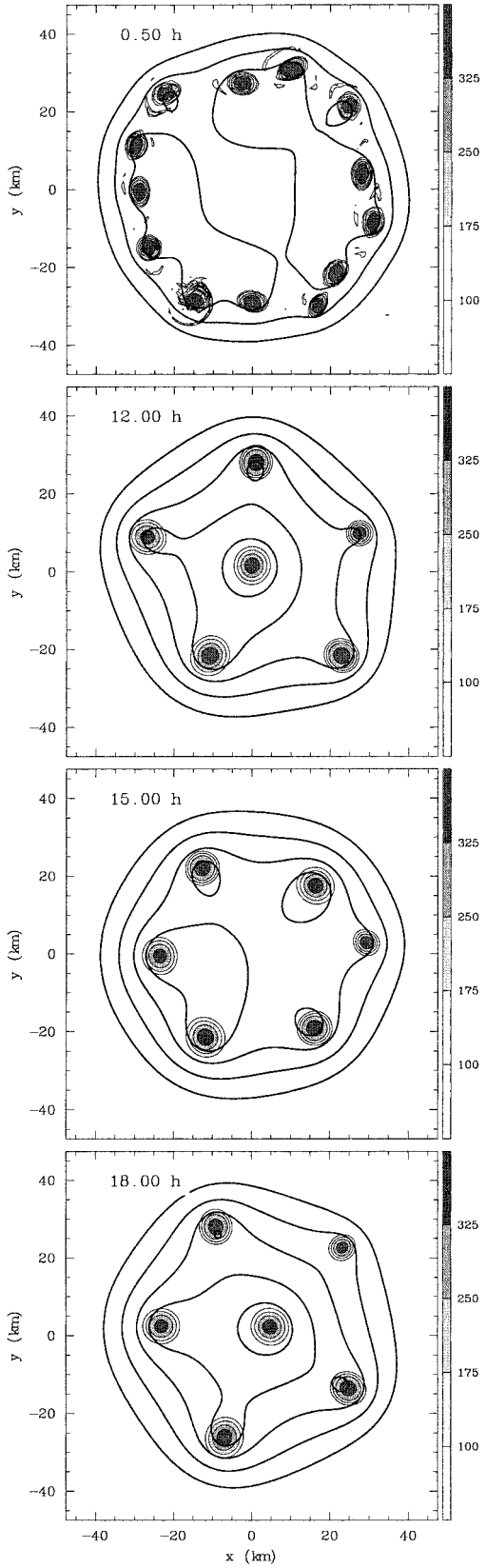

space we have explored in section 2, with the goal of drawing analogies to observed hurricane features. A more systematic exploration of this parameter space in the context of crystal (and monopole) formation would be beneficial, but a pseudospectral model, applied within our present limitations of grid resolution, may not be an ideal choice for such an exploration due to the inclusion of viscosity in (1). As discussed by Schecter et al. (1999), the presence of viscosity serves to increase the size of the mesovortices over time, thus reducing their resistance to merger. For a given viscosity, this effect becomes increasingly significant as the vorticity of the mesovortices, which depends on the initial vorticity of the annulus, is reduced. Thus a more complete systematic exploration may be better performed using inviscid methods, and is left here for possible future work. It is useful, however, to discuss the sensitivity of our results to viscosity, and we will do that here. Before we proceed, it should be noted that the removal, by diffusion, of finescale vorticity filaments has little effect on the pressure field since the pressure is related to vorticity by the smoothing operator ∇^{-2}.

In Exps. 1–7, calculations were performed (after dealiasing) using 170 × 170 Fourier modes on a 200 km × 200 km grid. For the viscosity value $\nu = 5\ \mathrm{m^2\ s^{-1}}$, the resulting 1/*e* damping time for modes having total wavenumber 170 was ~117 min. To test the sensitivity of our results to viscosity, we performed two additional experiments, based on the same initial conditions of expt. 2. For the first (expt. 8), we increased ν from 5 to 25 $\mathrm{m^2\ s^{-1}}$. This reduced the damping time, for modes with total wavenumber 170, by a factor of 1/5 to ~23 min. The vorticity and pressure evolution of expt. 8 was similar to expt. 2 and resulted in a minimum pressure of −27.3 mb. This minimum occurred at $t \approx 5$ h during monopole formation. After $t = 5$ h, the diffusive effects on the monopole cause the minimum pressure to increase at a rate of about 0.26 mb $\mathrm{h^{-1}}$. The minimum pressure during expt. 2 was −29 mb and occurred at $t = 5.5$ h. After $t = 5.5$ h, diffusion caused the minimum pressure to increase at about 0.04 mb $\mathrm{h^{-1}}$.

For the next experiment (expt. 9), we increased the spatial resolution of the model to 1024 × 1024 collocation points, resulting in 340 × 340 Fourier modes after dealiasing. The viscosity was reduced by a factor of 4 to $\nu = 1.25\ \mathrm{m^2\ s^{-1}}$, which resulted in a ~117 min damping time for modes having total wavenumber 340, but the damping time for modes with total wavenumber 170 was increased to ~7.8 h. Similarly to expt. 2, the

←

FIG. 9. Vorticity (shaded) and streamfunction contours (bold) for expt. 6. Here the inner 95 km × 95 km of the total domain is shown. Values along the label bar are in units of $10^{-4}\ \mathrm{s^{-1}}$. The shape of the streamlines transitions from a pentagon to a hexagon and back to a pentagon over 6 h.

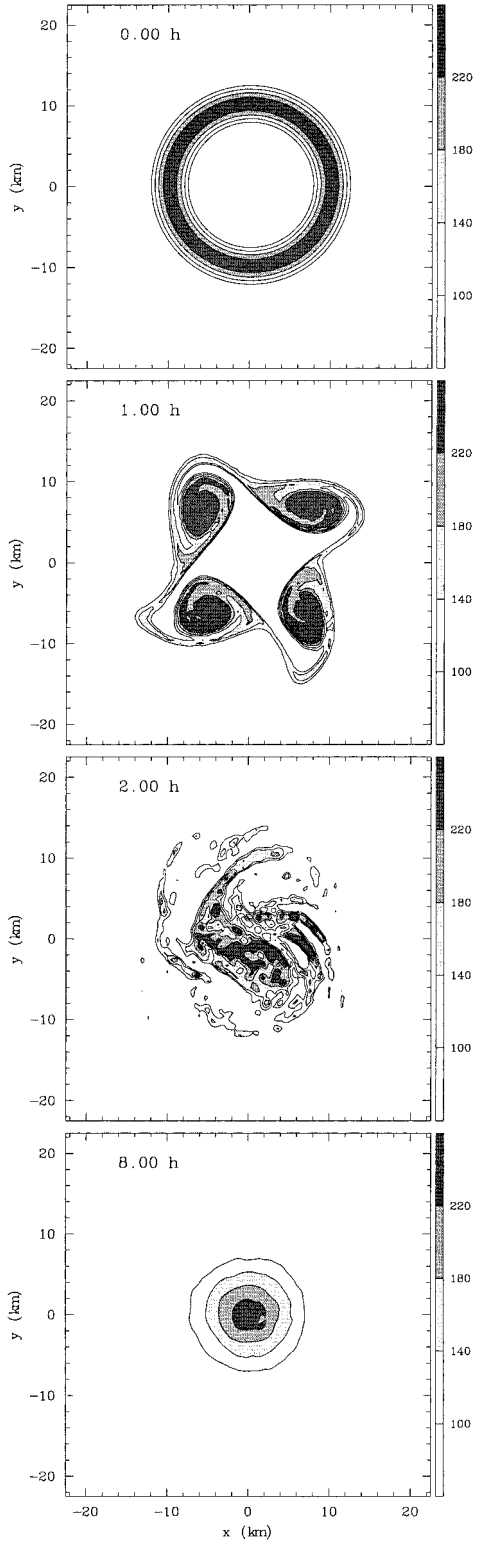

FIG. 10. Vorticity contour plots for expt. 7. The initial annulus rapidly relaxes to a monopole.

minimum pressure during expt. 9 was −29 mb and occurred around $t = 5$ h during monopole formation.

Based on the results of expts. 8 and 9, we conclude that the sensitivity to viscosity, of the evolution of minimum pressure, is negligible. Furthermore, although details of the 2D vorticity evolution, including the formation of a monopole or crystal, can artificially depend on diffusion, the main points of this work remain largely unaffected by viscosity. For example, a vortex crystal placed under the influence of viscosity will eventually collapse to a monopolar vorticity distribution, but for timescales appropriate to hurricanes, an asymmetric configuration that persists for just a few hours is significant. Of course, when considering the highly nonconservative flows of hurricanes, the evolution of vorticity, and the longtime behavior of mesovortices, would depend on many factors, other than viscosity, which are not considered in our simple framework.

3. Conclusions

This work has extended the findings of Schubert et al. (1999) and Montgomery et al. (2000) by considering the numerical evolution of hurricane-like vortices in which the eyewalls are initially represented by very thin annuli of enhanced vorticity surrounded by nearly irrotational flow. Such vorticity distributions more closely imitate observed vorticity profiles in intense or intensifying hurricanes.

Working with a 2D barotropic numerical model, we found that a number of remarkable features emerged during numerical integration of such initial conditions. The thin annuli quickly rolled up into mesovortices that underwent merger processes but did not typically consolidate rapidly into monopoles. Instead, the merger processes resulted in configurations of mesovortices that were maintained for many rotation periods. In some cases, the mesovortex configurations were steady and could be maintained for an indefinite number of rotation periods. The flows associated with such mesovortex configurations typically followed a number of straight line segments that gave the streamlines a polygonal appearance. These patterns evolved as the mesovortex configurations evolved, and bore strong resemblance to radar reflectivity patterns observed in intensifying hurricanes.

Local pressure perturbations as low as −50 mb were associated with the mesovortices. It is remarkable that such pressure falls can be realized solely through the mechanism of vorticity rearrangement in the absence of moist processes. In cases where the mesovortices eventually merged to form a monopole, the tangential flow in the eye increased substantially and the central pressure falls were as great as ~50 mb although the maximum tangential winds were found to decrease.

Based on a group of experiments in the idealized 2D barotropic framework, we suggest that the observed presence of radially thin regions of enhanced eyewall

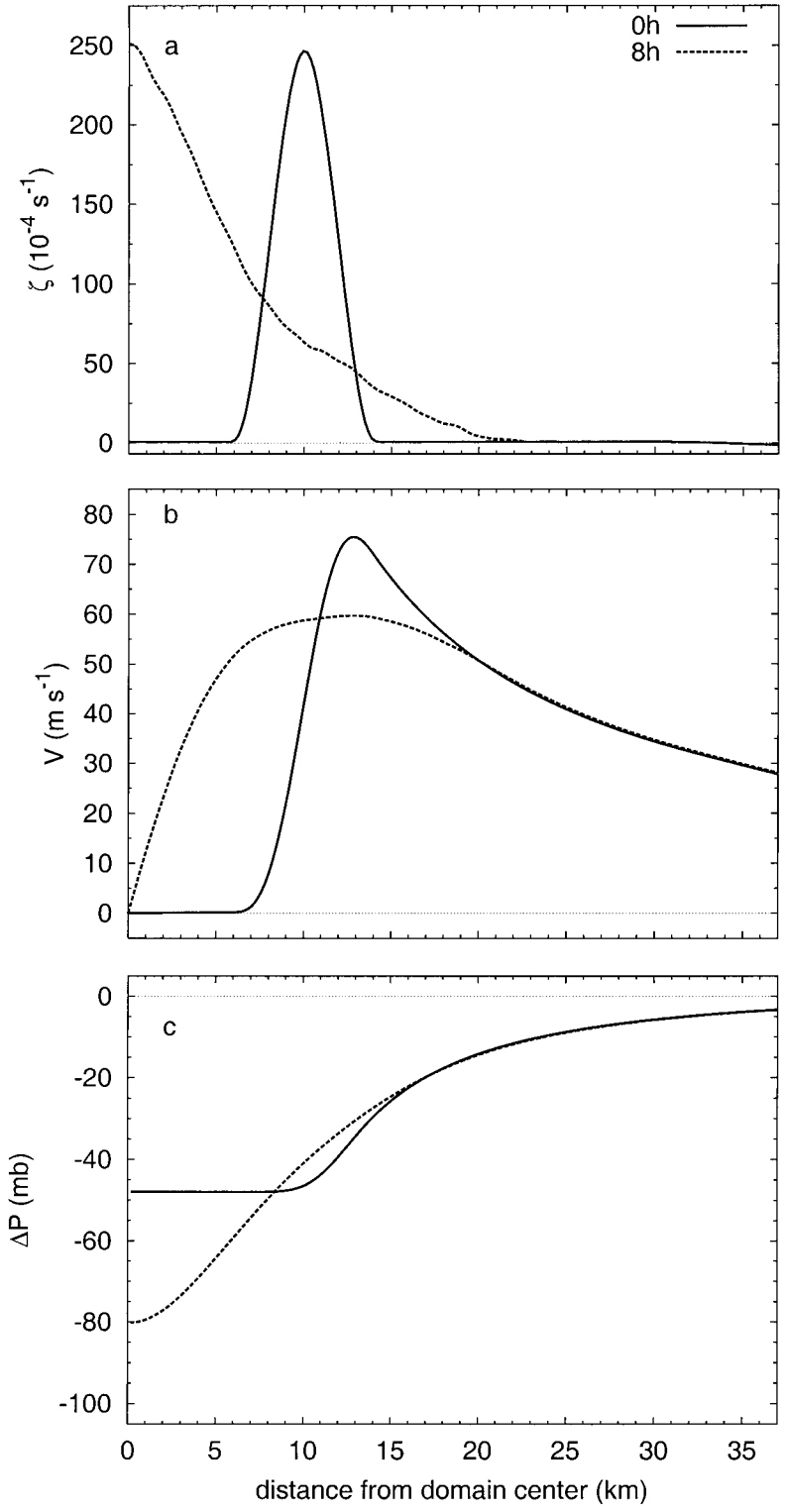

FIG. 11. Similar to Fig. 7 but for expt. 7. Note that the maximum vorticity at $t = 8$ h has not decreased from its initial value, indicating that very little mixing of the vorticity in the mesovortices with the surrounding low-vorticity fluid has occurred during the vorticity redistribution.

vorticity surrounding a nearly irrotational eye may be a precursory signature for rapid deepeding. The amount of expected deepening might be predicted based on the observed magnitude and structure of the enhanced eyewall vorticity.

Acknowledgments. We would like to thank Ricardo Prieto, Dave Nolan, Frank Marks, John Knaff, Matt Eastin, Todd Kimberlain, Michael Montgomery, Mark DeMaria, Ray Zehr, and Paul Reasor for their comments and assistance. This work was supported by NSF Grants ATM-9729970 and ATM-0087072 and by NOAA Grant NA67RJ0152 (Amendment 19).

REFERENCES

Black, P. G., and F. D. Marks, 1991: The structure of an eyewall meso-vortex in Hurricane Hugo (1989). Preprints, *19th Conf. on Hurricanes and Tropical Meteorology*, Miami, FL, Amer. Meteor. Soc., 579–582.

Bluestein, H. B., and F. D. Marks, 1987: On the structure of the eyewall of Hurricane Diana (1984): Comparison of radar and visual characteristics. *Mon. Wea. Rev.,* **115,** 2542–2552.

Bracco, A., J. C. McWilliams, G. Murante, A. Provenzale, and J. B. Weiss, 2000: Revisiting freely decaying two-dimensional turbulence at millennial resolution. *Phys. Fluids,* **12,** 2931–2941.

Carnevale, G. F., P. Cavazza, P. Orlandi, and R. Purini, 1991a: An explanation for anomalous vortex merger in rotating-tank experiments. *Phys. Fluids A,* **3,** 1411–1415.

——, J. C. McWilliams, Y. Pompeau, J. B. Weiss, and W. R. Young, 1991b: Evolution of vortex statistics in two-dimensional turbulence. *Phys. Rev. Lett.,* **66,** 2735–2737.

Dritschel, D. G., 1985: The stability and energetics of corotating uniform vortices. *J. Fluid Mech.,* **157,** 95–134.

——, 1988: Contour surgery: A topological reconnection scheme for extended integrations using contour dynamics. *J. Comput. Phys.,* **77,** 240–266.

——, 1998: On the persistence of non-axisymmetric vortices in inviscid two-dimensional flows. *J. Fluid Mech.,* **371,** 141–155.

Durkin, D. R., and J. Fajans, 2000: Experiments on two-dimensional vortex patterns. *Phys. Fluids,* **12,** 289–293.

Emanuel, K. A., 1997: Some aspects of hurricane inner-core dynamics and energetics. *J. Atmos. Sci.,* **54,** 1014–1026.

Fine, K. S., C. F. Driscoll, J. H. Malmberg, and T. B. Mitchell, 1991: Measurements of symmetric vortex merger. *Phys. Rev. Lett.,* **67,** 588–591.

——, A. C. Cass, W. G. Flynn, and C. F. Driscoll, 1995: Relaxation of 2D turbulence to vortex crystals. *Phys. Rev. Lett.,* **75,** 3277–3280.

Fletcher, R. D., J. R. Smith, and R. C. Bundgaard, 1961: Superior photographic reconnaissance of tropical cyclones. *Weatherwise,* **14,** 102–109.

Griffiths, R. W., and E. J. Hopfinger, 1987: Coalescing of geostrophic vortices. *J. Fluid Mech.,* **178,** 73–97.

Havelock, T. H., 1941: The stability of motion of rectilinear vortices in ring formation. *Philos. Mag.,* **11,** 617–633.

Jin, D. Z., and D. H. E. Dubin, 1998: Regional maximum entropy theory of vortex crystal formation. *Phys. Rev. Lett.,* **80,** 4434–4437.

Kossin, J. P., and M. D. Eastin, 2001: Two distinct regimes in the kinematic and thermodynamic structure of the hurricane eye and eyewall. *J. Atmos. Sci.,* **58,** 1079–1090.

——, W. H. Schubert, and M. T. Montgomery, 2000: Unstable interactions between a hurricane's primary eyewall and a secondary ring of enhanced vorticity. *J. Atmos. Sci.,* **57,** 3893–3917.

Lewis, B. M., and H. F. Hawkins, 1982: Polygonal eye walls and rainbands in hurricanes. *Bull. Amer. Meteor. Soc.,* **63,** 1294–1300.

Marks, F. D., Jr., and R. A. Houze Jr., 1984: Airborne Doppler radar observations in Hurricane Debby. *Bull. Amer. Meteor. Soc.,* **65,** 569–582.

——, and P. G. Black, 1990: Close encounter with an intense mesoscale vortex within Hurricane Hugo (September 15, 1989). *Extended Abstracts, Fourth Conf. on Mesoscale Processes,* Boulder, CO, Amer. Meteor. Soc., 114–115.

Melander, M. V., N. J. Zabusky, and J. C. McWilliams, 1988: Symmetric vortex merger in two dimensions: Causes and conditions. *J. Fluid Mech.,* **195,** 303–340.

Montgomery, M. T., J. M. Hidalgo, and P. D. Reasor, 2000: A semi-spectral numerical method for modeling the vorticity dynamics of the near-core of hurricane-like vortices. Atmospheric Science Paper 695, Dept. of Atmospheric Science, Colorado State University, 56 pp. [Available from Dept. of Atmospheric Science, Colorado State University, Fort Collins, CO 80523.]

Moore, D. W., and P. G. Saffman, 1975: The density of organized vortices in a turbulent mixing layer. *J. Fluid Mech.,* **69,** 465–473.

Morikawa, G. K., and E. V. Swenson, 1971: Interacting motion of rectilinear geostrophic vortices. *Phys. Fluids,* **14,** 1058–1073.

Muramatsu, T., 1986: The structure of polygonal eye of a typhoon. *J. Meteor. Soc. Japan,* **64,** 913–921.

Overman, E. A., and N. J. Zabusky, 1982: Evolution and merger of isolated vortex structures. *Phys. Fluids,* **25,** 1297–1305.

Persing, J., and M. T. Montgomery, 1995: A point-vortex application to vortex stability, evolution, and statistical equilibrium. Atmospheric Science Paper 587, Dept. of Atmospheric Science, Colorado State University, 86 pp. [Available from Dept. of Atmospheric Science, Colorado State University, Fort Collins, CO 80523.]

Peurrung, A. J., and J. Fajans, 1993: Experimental dynamics of an annulus of vorticity in a pure electron plasma. *Phys. Fluids A,* **5,** 493–499.

Saffman, P. G., and R. Szeto, 1980: Equilibrium shapes of a pair of uniform vortices. *Phys. Fluids,* **23,** 2339–2342.

Schecter, D. A., D. H. E. Dubin, K. S. Fine, and C. F. Driscoll, 1999: Vortex crystals from 2D flow: Experiment and simulation. *Phys. Fluids,* **11,** 905–914.

Schubert, W. H., M. T. Montgomery, R. K. Taft, T. A. Guinn, S. R. Fulton, J. P. Kossin, and J. P. Edwards, 1999: Polygonal eyewalls, asymmetric eye contraction, and potential vorticity mixing in hurricanes. *J. Atmos. Sci.,* **56,** 1197–1223.

Stewart, H. J., 1943: Periodic properties of the semi-permanent atmospheric pressure systems. *Quart. Appl. Math.,* **51,** 262–267.

Thomson, J. J., 1883: *A Treatise on the Motion of Vortex Rings.* Reprint, 1968, Dawsons of Pall Mall, 124 pp.

Willoughby, H. E., and P. G. Black, 1996: Hurricane Andrew in Florida: Dynamics of a disaster. *Bull. Amer. Meteor. Soc.,* **77,** 543–549.

——, J. A. Clos, and M. G. Shoreibah, 1982: Concentric eyewalls, secondary wind maxima, and the evolution of the hurricane vortex. *J. Atmos. Sci.,* **39,** 395–411.

Zabusky, N. J., and E. A. Overman, 1983: Regularization of contour dynamical algorithms. *J. Comput. Phys.,* **52,** 351–373.

——, M. H. Hughes, and K. V. Roberts, 1979: Contour dynamics for the Euler equations in two dimensions. *J. Comput. Phys.,* **30,** 96–106.